American Journal of Mechanical Engineering, 2017, Vol. 5, No. 5, 211-222
Available online at http://pubs.sciepub.com/ajme/5/5/4

DOI:10.12691/ajme-5-5-4

How Surface Roughness Performance of Printed Parts Manufactured by Desktop FDM 3D Printer with PLA+ is Influenced by Measuring Direction

Mohammad S. Alsoufi*, Abdulrhman E. Elsayed

Department of Mechanical Engineering, College of Engineering and Islamic Architecture, Umm Al-Qura University, Makkah, KSA
*Corresponding author: mssoufi@uqu.edu.sa

Abstract Design work related to the implementation of new elements requires the use of 3D CAD modelling techniques and rapid prototyping, which makes it possible to accelerate the deployment of new solutions significantly. In this paper, six successful assembly parts are 3D printed with advanced polylactic acid (PLA+) using the fused deposition modeling (FDM) method and are expressed by the arithmetic mean surface roughness, R_a. The surface roughness was measured in three different angular directions 0º, 45º and 90º during the investigation along with various independent process parameters of nozzle diameter (0.5, 0.3, 0.2 mm), layer height (0.3, 0.2, 0.1 mm) and other dependent variables, i.e., nozzle temperature (220°C), print speed (30 mm/s) and infill density (0%). Experimental results show that nozzle diameter and layer height play a major role in terms of part quality finish, build time and ultimately part cost. Nozzle diameter and a layer height of 0.3 mm and 0.1 mm, respectively, represent the optimal manufacturing process parameters that can be selected. The surface roughness behaviour does not change and remains relatively constant and follows a similar trend with minor variations for both 45° and 90° measuring angle. Whereas, the surface roughness values are susceptible to 0° measuring direction to the build orientation as compared to other angles.

Keywords: *3D, polylactic acid (PLA+), fused deposition modeling (FDM), surface roughness*

Cite This Article: Mohammad S. Alsoufi, and Abdulrhman E. Elsayed, "How Surface Roughness Performance of Printed Parts Manufactured by Desktop FDM 3D Printer with PLA+ is Influenced by Measuring Direction." *American Journal of Mechanical Engineering*, vol. 5, no. 5 (2017): 211-222. doi: 10.12691/ajme-5-5-4.

1. Introduction

Increased competitiveness in the marketplace including micro- and nano-devices has forced production companies into a faster product development and reduction of new product implementation time to market [1]. To stay competitive in the marketplace, manufacturers need to set up to achieve and sustain themselves by their creativity as 'world class manufacturers' (WCM). Among various manufacturing technologies, 3D printing technology, or its other synonyms such as additive manufacturing (AM), solid free form (SFF) or rapid prototyping (RP), is a process of joining the material technique used to create an object/part from three-dimensional (3D) digital model data, usually layer-by-layer (layer manufacturing), without tools, die casting, fixtures or even human intervention [2], which was first described in 1986 by Charles Hull and commercialized in 1990 as RP technology [3]. This technology creates an object/part by adding engineering materials rather than removing materials in order to reduce waste while reaching a satisfactory surface finish quality item [4] with a significant reduction in manufacturing cost due to the absence of tooling [5] and has grown substantially in both volume and scope [6,7]. Additive manufacturing (AM) technologies available commercially include stereolithography (STL) [8], selective laser sintering (SLS) [9], inkjet printing (IJP) [10], direct metal deposition (DMD) [11] and fused deposition modelling (FDM) [12]. A widely used technique of RP involving fused deposition modeling (FDM), also known as fused filament fabrication (FFF) or molten polymer deposition (MPD), however, has already existed since the '80s.

In the FDM manufacturing process, as shown in Figure 1, a circular nozzle, typically 1.70 mm in diameter, that transverses in *x* and *y* planes by multi-speed numerical controlled mechanism, is directly controlled by computer aided manufacturing (CAM) to generate each two-dimensional (2D) layer of about 20 µm to 300 µm (this depends on 3D printer and process parameters) and extrude these from a spool thermoplastic filament material or composites with thermoplastic materials to semi-molten state processes [2,13]. The spooled thermoplastic filament materials are fed into the liquefier through a set of two mechanical freewheels driven in a counter rotating mode, which delivers enough torque to the thermoplastic filament material to perform as a piston during the extrusion stage and then deposit it layer-by-layer or path-by-path based on the 3D computer aided design (CAD) model onto an adjustable build platform [14]. The build platform holding the 3D printed sample then moves vertically downwards in the *z* plane to commence depositing a new layer/path on top of the previous one.

After a period, the print head nozzle will have deposited a complete physical description of the original three-dimensional (3D) computer aided design (CAD) design file [15].

The material platform for FDM 3D is continuously increasing in order to enhance the applicability of FDM-type [16]. However, the available engineering materials are generally limited to thermoplastics and/or composites with thermoplastic, such as polycarbonate (PC), polylactic acid (PLA), polyphenylsulfone (PPSF or PPSU), acrylonitrile butadiene styrene (ABS) and so on [17, 18], due to their stable thermomechanical properties and excellent chemical resistance. Likewise, many commercial FDM extruders are restricted to a nozzle temperature of up to 300°C, this makes the extruded thermoplastic filament material to re-solidify upon deposition on the build platform, and also in order to ensure that the printed layers/paths do not lose geometry from the original 3D model [19]. Recently, bio-degradable thermoplastic polymers such as polylactic acid (PLA) have been used instead of conventional thermoplastic polymers for a number of reasons including an excellent environmental impact. It has high Young's modulus in the range of 2 GPa to 3 GPa and tensile strength in the range of 50 MPa to 70 MPa which is comparable to that of petroleum based plastic. On the other hand, it is very brittle and has only low toughness [20]. Commonly, PLA is used as medical applications, containers, packages, automobile components and so on [21].

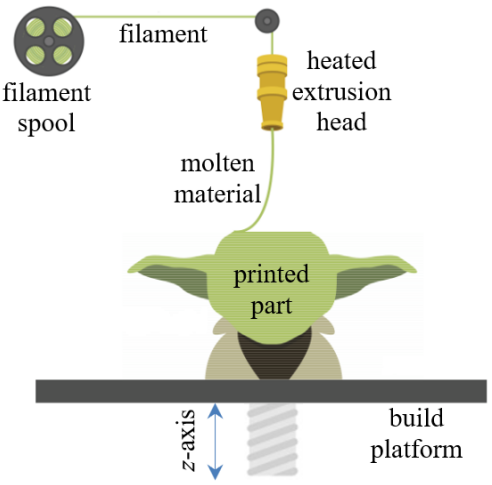

Figure 1. FDM process

Figure 2. Generalized AM process steps

The FDM 3D manufacturing process involves a series of steps as shown in Figure 2. To address this issue, start with a 3D CAD model file either by creating or scanning the 3D model. CATIA® V5 R20 software is used for the 3D model using CAD module of the CAD/CAM system. The 3D model design is then converted to an STL (Stereolithography or Standard Triangulated Language) file using CATIA itself. The KISSlicer software (version 1.6) slices STL files into printer-ready G-code (geometric code) files and a G-code is then generated which controls the extrusion head of the desktop FDM 3D printer.

1.1. Proposed Approach

Surface finish quality is crucial not only for improved functionality and appearance but also for cost-effectiveness and overall prototyping time reduction. As the AM process is performed using a layered manufacturing technique, one of the most important disadvantages of FDM is that the surface roughness of the printed part is excessively rough, especially when compared to other processes. The poor surface finish quality observed in end products of the FDM process has mainly been due to the layer upon layer deposition of the building process and is also influenced by tessellation of the original CAD model. A precise characterization of surface roughness is of prime importance in many engineering industries. For this reason, the surface roughness, R_a, is a key issue in AM. To ensure better surface integrity, attention must be given to the selection of the manufacturing process parameters and measuring direction. Within this research paper, two essential questions will be considered that help to answer the following main research questions:

- How is the surface roughness, R_a, influenced by independent manufacturing process parameters (i.e., nozzle diameter and layer height) of the desktop FDM 3D printer technology?
- How is the surface roughness, R_a, influenced by the different measuring angle (0°, 45°, 90°)?

2. Experimental Methodology

2.1. 3D Printer and Printing Material

For the purposes of this investigation, the desktop FDM 3D printer (do-it-yourself kit) was used based on an open source digital model known as 'The BEAST', (available from Cultivate3D, Australia). For more details about the basic technical details, see [22]. This printer is a fully customized desktop 3D printer which allows lightweight, cost-effective, and very rapid prototyping (RP) compared to conventional machining (i.e., CNC machine).

The long-fiber thermoplastic filament material used in this study for model fabrication was commercially available which is advanced polylactic acid, PLA+, (eSUN PLA+ filament, the advanced formula by added additional bio-polyester blends), light blue coloured, 1.75 mm in diameter and showed ±0.05 mm tolerance (purchased from Shenzhen Esun Industrial Co., Ltd.). It was selected because of its green environmental reputation, bio-compostability (bio-based plastic), agreeable aroma as well as its low warping deformation and excellent printed part quality, with the molecular formula $(C_3H_4O_2)_n$.

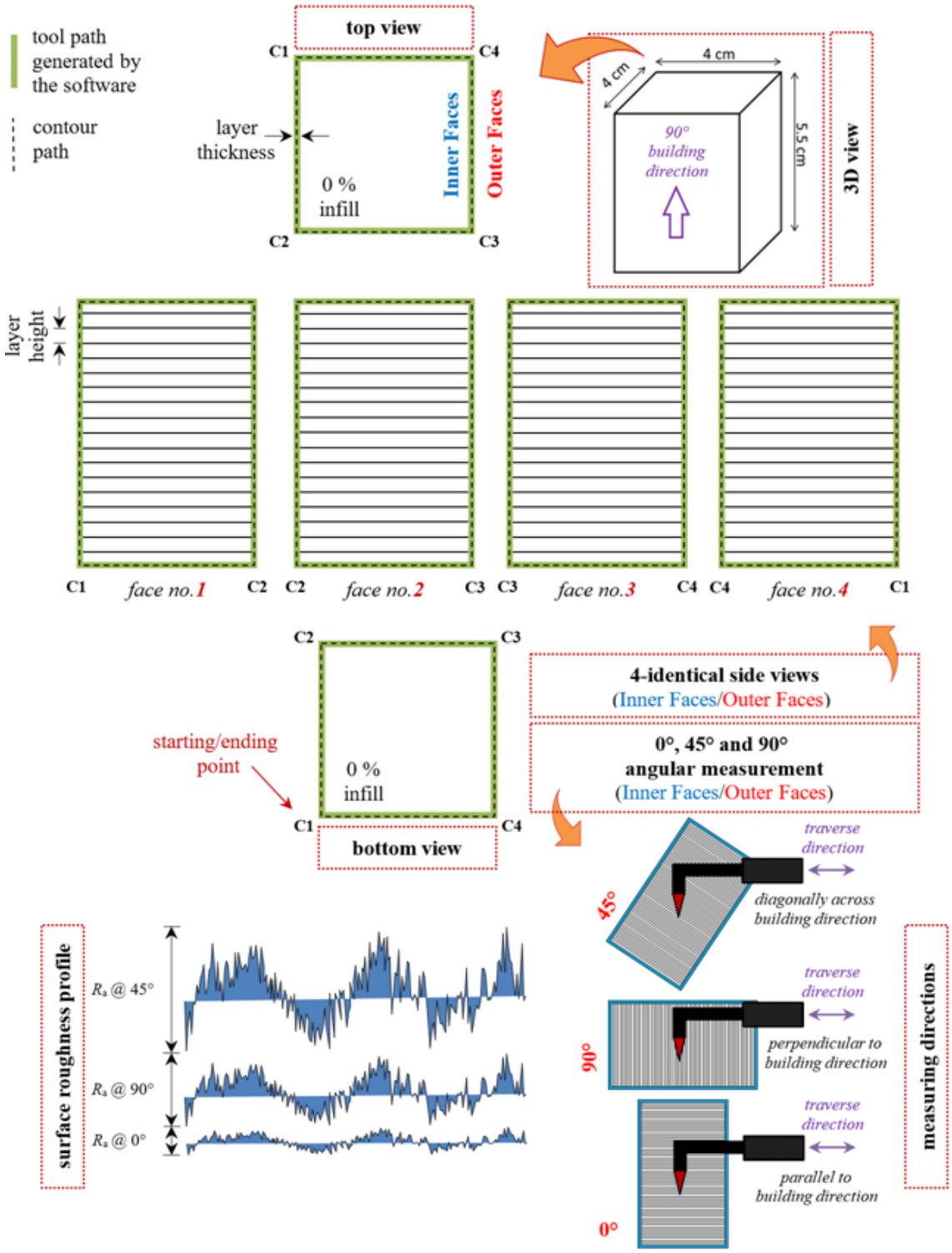

Figure 3. Proposed framework of the 0% infill density with inner and outer faces and measuring direction

2.2. Printing Process Parameters

In FDM 3D, there are many processing parameters that can be controlled and may affect the properties of the printed part. The effects of printing process parameters have been comprehensively researched. These printing process parameters include nozzle temperature [23,24], print bed and ambient room temperatures [23], print speed [24], print orientation [25,26,27], layer-to-layer orientation [26,28], layer height [26], filament material diameter [29], circular nozzle diameter and air gap [26] and filament material composition [29,30,31]. In this work, after conducting a great many test trials in order to understand the capabilities, limitations, and problems of the desktop FDM 3D printer, three different nozzle diameters, and layer heights are taken into consideration as independent variables, whereas other dependent process parameters of the operating setup of the desktop FDM 3D printer can be illustrated in Table 1. Bear in mind, the desktop FDM 3D printer process parameters were identified from a previous study reported in [22] and also based on the knowledge and experience of the researchers.

Table 1. Summary of the operating setup of the personal FDM 3D printer

Parameters	Values
Filament Material	PLA+
Colour	Light Blue
AM Process	FDM (Fused Deposition Modeling)
Layer Height (mm)	0.3, 0.2, 0.1
Infill Density (%)	0
Nozzle Diameter (mm)	0.5, 0.3, 0.2
Nozzle Temperature (°C)	220
Printing Speed (mm/s)	30
Extrusion of Material (layer width) (mm)	0.48
Speed for non-print moves (mm)	60
Horizontal Shells (top and bottom layer)	0
Vertical Shells	1
Cooling Rate	build-in
Bed Temperature (°C)	Room Temperature
Room Temperature (°C)	25±1
Relative Humidity (% RH)	40±5

2.3. FDM Printed Parts

To demonstrate the proposed fabrication technology, which allows lightweight, low-cost, and very rapid/easy prototyping compared to conventional machining such as CNC machine, six FDM 3D printed parts were successfully fabricated one at a time layer-by-layer using PLA+ thermoplastic filament material, as shown in Figure 4, at an independent nozzle diameter of 0.5, 0.3, 0.2 mm and layer height of 03, 0.2, 0.1 mm. All other printing process parameters were kept constant between prints. The infill density for FDM 3D printed parts is selected at the lowest practical level in order to save print time and filament material. So, the infill density was set at 0% with only one vertical shell. Then, the fabricating part was carried out on the top of a glass platform (flat build orientation with 0/90 printing raster direction) that underneath has no heating bed and stands in an air-conditioned room temperature of 25±1°C and relative humidity of 40±5% RH. To control the ambient temperature effects, the print space could equilibrate at 25±1°C before the start of printing. The weight and time spent of fabrication of the proposed six FDM 3D printed part with 0% infill density are illustrated in Table 2. It is worth mentioning that it was decided that this would be kept very simple regarding geometry to enable the subsequent measurements: 40 mm (L) × 40 mm (W) × 55 mm (H) square. Only 3D samples from builds in which all samples printed successfully were used for testing and analysis.

As can be seen from Table 2, printed parts with a greater layer height (0.3 mm) will, therefore, have less accuracy and detail in print than prints with a lower layer height (0.2 or 0.1 mm). However, printing with a low layer height (0.1 mm) will take much longer to print (1h:57m:18s) and require more thermoplastic filament material and increase the cost of the printed part.

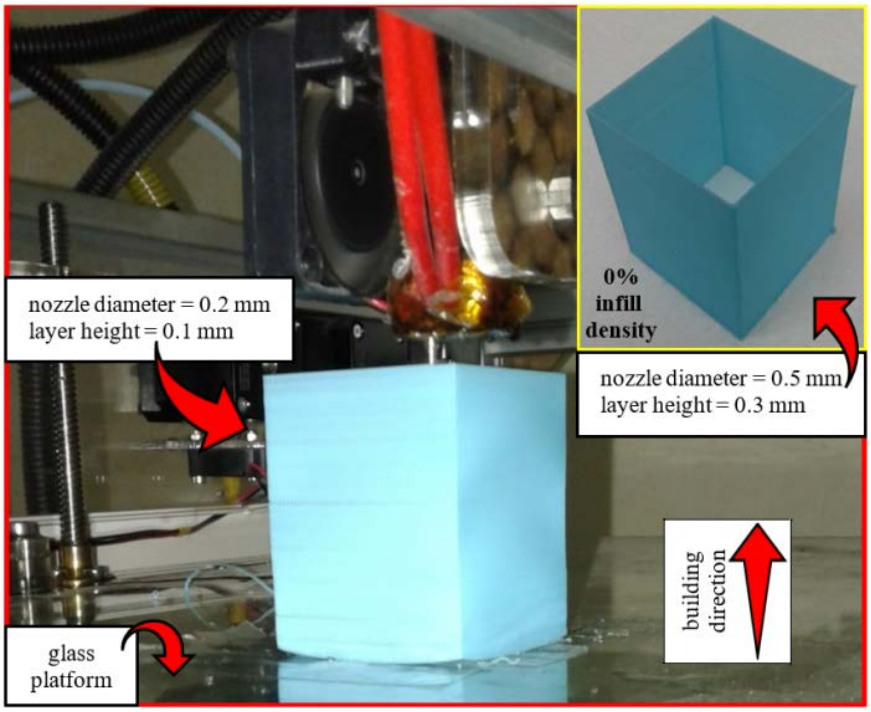

Figure 4. FDM 3D printed part

Table 2. Weight and time of fabricated printed parts

Printed Part No.	**1**	**2**	**3**	**4**	**5**	**6**
Nozzle Diameter (mm)	0.5	0.5	0.5	0.3	0.3	0.2
Layer Height (mm)	0.3	0.2	0.1	0.2	0.1	0.1
Weight (g)	5.9682	5.9116	6.1200	3.4686	3.7312	2.3436
Time	38m:57s	58m:32s	1h:56m:25s	58m:40s	1h:57m:1s	1h:57m:18s

2.4. Testing Equipment

With an optimal combination of low contact force of 0.7 mN, high displacement sensitivity of 50 nm and the small tip radius of a 2 µm stylus being used in this study, the distribution of surface potential irregularities of the 0% infill density printed specimen was measured using a conventional contact-type Taly-Surf® profilometer from Taylor Hobson Precision, Inc. The examinations were performed under the essentially wear-free concept and high-precision position measurement, which offered high resolution down to 0.8 nm, a measuring range (*x*-axis) of 12.5 mm, and linear speed up to 0.5 mm/s. The traces were auto-levelled and set-up to a linear least-squares (LLS) straight line and then filtered with a standard low-pass of 0.8 mm cut-off wavelength. More details of the surface roughness measurement procedure have been reported elsewhere [32-41].

The contact-type profilometer was calibrated before taking measurements. For convenience, a series of ten calibration trials have been carried out using an international standard ball of 22.0161 mm diameter as a reference (from Taylor Hobson Precision, Ltd.). Calibration results showed that the cantilever beam system at only one end was a linear mass-spring system ($R^2 > 0.999$) under operational and environmental conditions, with an absolute uncertainties value of <1% and measurement resolution down to at worst 50 nm. This result is adequate as these trials are predominantly about related behaviour; design interpretation to other systems is always vulnerable to variations in materials and dimensions.

2.5. Statistical Analysis

The surface roughness measurement was conducted in the middle zone per each face (four-identical faces). It is worth mentioning that C1 (corner no.1) represents the starting point of the printing process, whereas C4 (corner no.4) represents the end point of the printing process. So, C1 to C2 represents face no.1, C2 to C3 represents face no.2, C3 to C4 represents face no.3, and finally, C4 to C1 represents face no. 4 for both inner and outer faces indicating a total of 8 points to be measured per one printed part. A total of 144 points are to be measured (72 points in the outer four identical faces and another 72 points in the inner four identical faces).

In this paper, the surface roughness, R_a, was measured off-line quantitatively in µm from the filtered profiles. The surface roughness amplitude parameter was selected according to the recommendations in the literature review and with consideration of the data processing facilities available with differing levels of information [42,43,44,45,46]. The obtained data were reviewed and analyzed qualitatively with OriginLab® 2017 software. The measurement and resultant assessment of the desired FDM 3D printed part was successfully carried out according to international standards. The surfaces are measured three times along a distance of 10 mm in the middle zone per each face (inner and outer 4-identical faces), and the average is taken as an output.

3. Experimental Results and Discussion

Six samples were printed one at a time for surface roughness testing and analysis using a double-sided adhesive on the glass platform to avoid the warping issue. Then, all printed parts were cooled down to an ambient room temperature 25±1°C. After that, the 0% infill density printed part was removed from the glass platform, and the measurement performance was conducted for all inner and outer faces in the middle zone (around 15 to 20 mm from either the bottom or the top of the printed part) and the average values were considered. Deviation from each measurement is calculated and presented in the form of mean and standard deviation (mean±SD). All FDM 3D printed part surface roughness was measured in three different angular positions of 0°, 45° and 90° to build direction (from bottom to top). The surface finish of the specimens is obtained by using a contact-type roughness tester. The experimental observations are discussed in the following section.

Table 3 includes the surface roughness response of all inner faces at 0°, 45° and 90° measuring angles along with the mean and standard deviation for all six FDM 3D printed parts. Whereas, Table 4 includes the surface roughness response of all outer faces at 0°, 45° and 90° measuring angles along with the mean and standard deviation for all six FDM 3D printed parts. For both Table 3 and Table 4, it could be observed that there is a steady increase in the surface roughness distribution as the layer height was being increased (from 0.1 mm to 0.3 mm) and hence the surface roughness could be said to be directly proportional to the layer height. Thus, whenever the best surface quality is desired, the selection of process parameters of layer height to be used in manufacturing must be very small.

3.1. Surface Roughness Profile

Figure 5, Figure 6, Figure 7 show the differences in the surface roughness behaviour profiles of printed parts at different angles (0°, 45°, 90°) over a 10 mm measuring distance. Figure 5(a) shows the surface roughness profile at a 0° measuring direction with frequent peaks to valleys distribution. Figure 6(a) shows the surface roughness profile at a 45° measuring direction with wider peaks to valleys distribution. Figure 7(a) shows the surface roughness profile at a 90° measuring direction with narrower peaks to valleys distribution. This indicates that the surface roughness values are susceptible to the measuring direction angle, θ. In general, the surface roughness increases with an increase in the measuring direction angle until 45º, with respect to the build direction of 90º and decreases later with an increase in the measuring direction angle until 90º. Between the 45° and 90° measuring direction, the surface roughness change remains relatively constant with minor variation.

The data generated from Figure 5(a) reveal that the surface behaviour distribution region is smooth, −3.111 µm < surface profile < +2.289 µm with a mean and standard deviation of 1.0233±1.2 µm at a 0° angle measuring direction. On the other hand, the data generated from Figure 6(a) and Figure 7(a) reveal that the surface behaviour distribution region is rough, −84.922 µm < surface profile < +49.501 µm with mean and standard deviation of 34.7293±40.2 µm at a 45° angle measuring direction and −85.934 µm < surface profile < +51.934 µm with mean and standard deviation of 31.9390±37.5 µm at 90° angle measuring direction.

Table 3. Surface roughness (inner faces)

Printed Part No.	Surface Roughness (μm)	Inner Faces				Mean	±SD
		Face No.1 (C1 - C2)	Face No.2 (C2 - C3)	Face No.3 (C3 - C4)	Face No.4 (C4 - C1)		
Nozzle Diameter = 0.5 mm and Layer Height = 0.3 mm							
1	R_a @ 0°	1.4446	1.344	1.6269	0.9773	1.35	0.27
	R_a @ 45°	37.0573	36.4608	37.633	36.7085	36.96	0.51
	R_a @ 90°	33.2943	32.6814	33.4522	31.7007	32.78	0.79
Nozzle Diameter = 0.5 mm and Layer Height = 0.2 mm							
2	R_a @ 0°	2.0394	2.0662	2.8696	1.2892	2.07	0.65
	R_a @ 45°	22.4323	21.8081	20.6335	28.9004	23.44	3.71
	R_a @ 90°	21.7547	20.904	19.7598	26.2476	22.17	2.84
Nozzle Diameter = 0.5 mm and Layer Height = 0.1 mm							
3	R_a @ 0°	1.7052	6.4298	6.2361	4.6017	4.74	2.19
	R_a @ 45°	15.7584	18.5059	14.029	12.0904	15.10	2.72
	R_a @ 90°	15.2823	14.4466	17.7515	15.4151	15.72	1.42
Nozzle Diameter = 0.3 mm and Layer Height = 0.2 mm							
4	R_a @ 0°	3.5095	4.1734	0.9037	1.824	2.60	1.50
	R_a @ 45°	22.7954	22.4523	24.671	24.0782	23.50	1.05
	R_a @ 90°	19.8834	20.4995	23.0288	21.4029	21.20	1.37
Nozzle Diameter = 0.3 mm and Layer Height = 0.1 mm							
5	R_a @ 0°	1.2727	1.0648	2.7133	2.2461	1.82	0.79
	R_a @ 45°	9.6827	9.108	9.519	8.9845	9.32	0.33
	R_a @ 90°	10.3648	8.456	10.0769	8.8718	9.44	0.92
Nozzle Diameter = 0.2 mm and Layer Height = 0.1 mm							
6	R_a @ 0°	3.1781	2.7073	3.4288	1.5152	2.71	0.85
	R_a @ 45°	8.4636	12.1485	9.6486	11.3253	10.40	1.66
	R_a @ 90°	7.8754	11.2575	9.7203	13.2168	10.52	2.27

Table 4. Surface roughness (outer faces)

Printed Part No.	Surface Roughness (μm)	Outer Faces				Mean	±SD
		Face No.1 (C1 - C2)	Face No.2 (C2 - C3)	Face No.3 (C3 - C4)	Face No.4 (C4 - C1)		
Nozzle Diameter = 0.5 mm and Layer Height = 0.3 mm							
1	R_a @ 0°	1.7636	0.962	1.269	0.9691	1.24	0.38
	R_a @ 45°	33.9348	34.1537	35.7264	35.9451	34.94	1.04
	R_a @ 90°	31.6403	31.6269	32.7856	32.5879	32.16	0.61
Nozzle Diameter = 0.5 mm and Layer Height = 0.2 mm							
2	R_a @ 0°	2.0719	2.122	1.8157	2.8238	2.21	0.43
	R_a @ 45°	29.1316	23.0083	22.005	30.7305	26.22	4.36
	R_a @ 90°	24.8075	21.269	20.6275	29.5439	24.06	4.09
Nozzle Diameter = 0.5 mm and Layer Height = 0.1 mm							
3	R_a @ 0°	2.9918	9.3055	11.8554	10.3374	8.62	3.90
	R_a @ 45°	20.4251	17.006	12.0769	13.7845	15.82	3.69
	R_a @ 90°	15.188	17.9636	15.0698	14.0192	15.56	1.69
Nozzle Diameter = 0.3 mm and Layer Height = 0.2 mm							
4	R_a @ 0°	1.0071	1.4998	0.813	0.9837	1.08	0.30
	R_a @ 45°	24.9486	24.9669	23.4345	22.5546	23.98	1.19
	R_a @ 90°	21.692	22.6099	21.7538	21.0817	21.78	0.63
Nozzle Diameter = 0.3 mm and Layer Height = 0.1 mm							
5	R_a @ 0°	1.268	0.7825	1.6042	1.5143	1.29	0.37
	R_a @ 45°	10.8355	9.8911	9.3991	9.783	9.98	0.61
	R_a @ 90°	8.2634	10.2928	8.6141	9.3617	9.13	0.90
Nozzle Diameter = 0.2 mm and Layer Height = 0.1 mm							
6	R_a @ 0°	1.851	2.5073	1.5842	0.734	1.67	0.73
	R_a @ 45°	9.4209	10.1548	14.0196	9.166	10.69	2.26
	R_a @ 90°	12.5693	11.0999	8.9528	8.2678	10.22	1.98

On the other hand, Figure 5(b), Figure 6(b), and Figure 7(b) show histograms of the distribution of vertices and upgrades located on the surface samples. It can be seen that the distribution of the 3D printed sample is characterized by a significant fluctuation of changes in the value of *R* group parameters and larger changes range values of these parameters. This proves that the surface of the printed sample has an undirected structure.

It provides the general trend of the third-order and fourth-order central moments of skewness, R_{sk}, (3^{rd} moment) and kurtosis, R_{ku}, (4^{th} moment). It shows that the general trend is negatively skewed distribution for skewness, R_{sk}, (3^{rd} moment) and 100% platykurtic distribution, heterogeneous, wide scatter and peaks are bumpy with a low degree of peakedness for the kurtosis, R_{ku}, (4^{th} moment), indicating that the manufactured parts were an almost full deposit of PLA+ thermoplastic filament material, whether the measuring direction was set at 0°, 45° and/or 90° angle measurements. It also means that the distribution for the kurtosis (4^{th} moment) with less than 3 produces fewer and less extreme outliers than does the normal distribution.

The ratio R_q/R_a performance (root means square, R_q, to average surface roughness, R_a) tends to follow the same pattern of approximately ~1.2±0.01 with only less than ~1.5% difference.

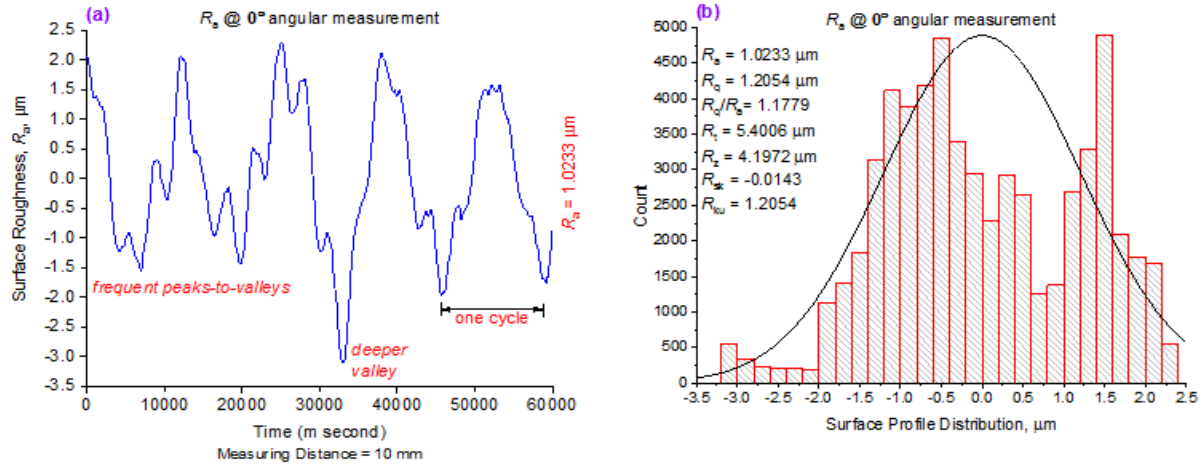

Figure 5. Surface roughness @ 0° (a) height profile and (b) distribution profile

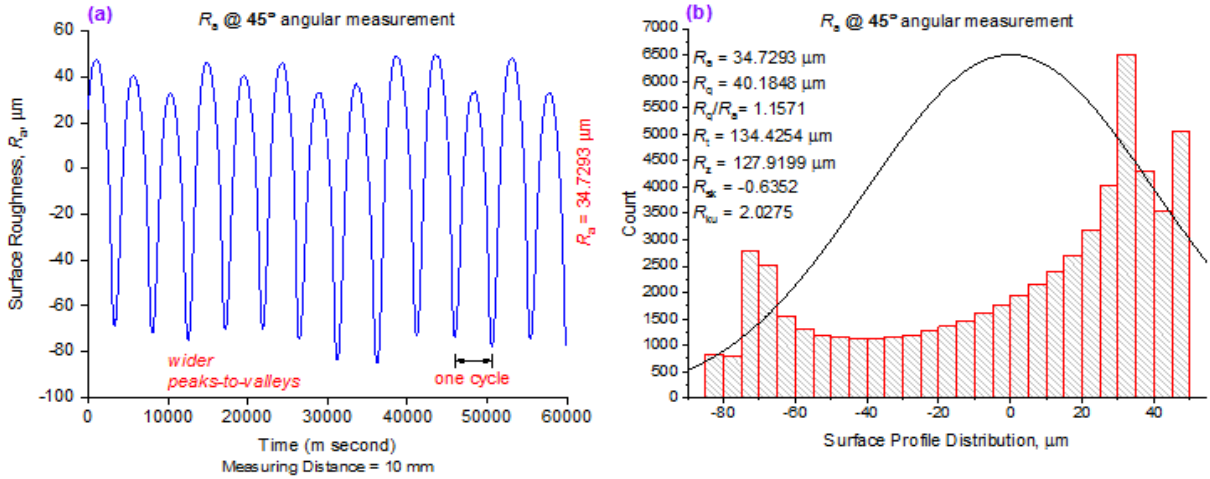

Figure 6. Surface roughness @ 45° (a) height profile and (b) distribution profile

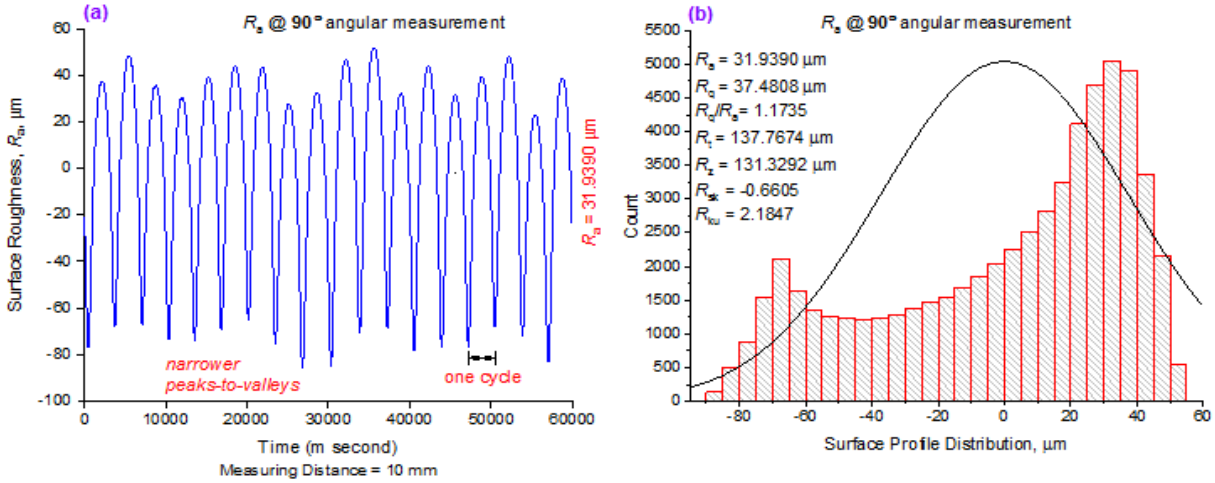

Figure 7. Surface roughness @ 90° (a) height profile and (b) distribution profile

3.2. Surface Roughness Behaviour at Inner Faces

Figure 8 shows a response surface graph for the effect of nozzle diameter (0.5, 0.3, 0.2 mm) and layer height (0.3, 0.2, 0.1 mm) as independent process parameters along with measuring direction (0°, 45°, 90°) on the surface roughness behaviour of six FDM 3D printed parts. The nozzle temperature settings were automatic and therefore all six FDM 3D printed parts were fabricated at the same temperature configuration of 220°C with 0% infill density. As can be seen from Figure 8, a nozzle diameter of 0.5 mm and a layer height of 0.3 mm represents the highest surface roughness among all 72 points (6 samples) at inner faces whereas a nozzle diameter of 0.3 mm and a layer height of 0.2 mm represents the lowest surface roughness among all 72 points (6 samples) at inner faces. As predicted, the thin layer height (0.1 mm) had produced a smoother surface than the thick layer height (0.3 mm) whether it was measured at 0°, 45° or 90° angle measurements.

The best surface roughness was obtained in printed part no.4 (face no.3), R_a = 0.9037 µm with a 0° angle measurement direction, where nozzle diameter and layer height were 0.3 mm and 0.2 mm, respectively. On the other hand, the worst surface roughness was obtained in printed part no.1 (face no.3) R_a = 37.633 µm with a 45° angle measurement direction, where nozzle diameter and layer height were 0.5 mm and 0.3 mm, respectively. With a minimum layer height of 0.2 mm, the surface roughness decreased significantly by almost 97.6%, and this is the best surface roughness behaviour in all six FDM 3D printed parts analysed. With a maximum layer height of 0.3 mm, the surface roughness increased significantly by almost four hundred times. This was because the maximum layer height of 0.3 mm required more time to cure for the crystallization of the thermoplastic filament material.

When measuring the direction of 45° (diagonally across building direction) and 90° (perpendicular to building direction), the difference of the surface roughness behaviour fluctuated within ~8 µm of one another. Whereas, when measuring the direction of 0° (parallel to building direction), the surface roughness behaviour fluctuated within ~3 µm.

At 0.5 mm nozzle diameter for both 45° and 90°, the surface roughness behaviour decreased by almost 37% indicating that the surface finish improved from ~40 µm (at 0.3 mm layer height) to ~25 µm (at 0.2 mm layer height) until it reached ~18 µm when the layer height is 0.1 mm. At 0.3 mm nozzle diameter for both 45° and 90°, the surface roughness decreased by almost 52% indicating that the surface finishes improved from ~25 µm (at 0.2 mm layer height) to ~12 µm (at 0.1 mm layer height). At 0.2 mm nozzle diameter for both 45° and 90°, the surface finish reached ~10 µm when the layer height is 0.1 mm. On the other hand, at 0° measuring direction, all surface roughness behaviour was approximately the same for all nozzle diameter and layer height at around ~3 µm, indicating that with 0° angle measurement (parallel to building direction), the independent manufacturing process parameters, i.e., nozzle diameter and layer height have no influence or very little influence on the surface roughness behaviour. The effect of nozzle diameter and layer height on the surface roughness can also be seen with naked-eye observation.

To conclude at inner faces (72 points), printed part no.6 represents the lowest average surface roughness behaviour with the absence of pits, holes, and irregularities. It also shows the same fluctuated surface roughness behaviour indicating that the layer height of 0.1 mm has more influence than the nozzle diameter whether it was measured at 0°, 45° or 90° angle measurements.

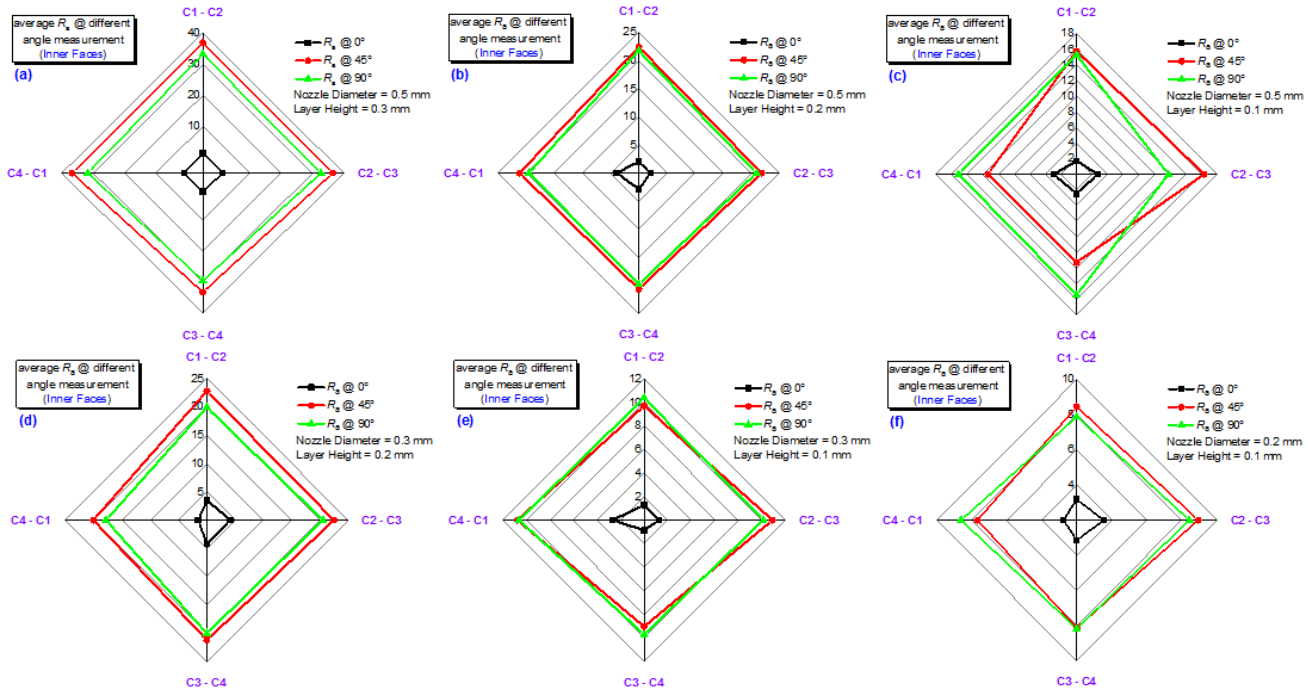

Figure 8. Surface roughness of inner faces at different angular measurement and different process parameters

3.3. Surface Roughness Performance at Outer Faces

The same analysis is done for the 72 points at outer faces. Figure 9 shows response surface graph for the effect of nozzle diameter (0.5, 0.3, 0.2 mm) and layer height (0.3, 0.2, 0.1 mm) as independent process parameters along with measuring direction (0°, 45°, 90°) on the surface roughness of six FDM 3D printed parts at outer faces. The nozzle temperature settings are automatic and therefore all six 3D FDM printed parts were fabricated at the same temperature configuration of 220°C with 0% infill density. As can be seen from Figure 9, a nozzle diameter of 0.5 mm and thick layer height of 0.3 mm represents the highest surface roughness (R_a = 35.9451 µm with a 45° angle measurement direction) at outer face no.4, whereas a nozzle diameter of 0.3 mm and layer height of 0.2 mm represents the lowest surface roughness (R_a = 0.813 µm with 0° angle measurement direction) at outer face no.3. These findings are consistent behaviour with the data obtained in Figure 7 for inner faces, whether it was measured at 0°, 45° or 90° angle measurements.

With a minimum layer height of 0.2 mm, the surface roughness behaviour decreased significantly by almost 97.7% and this is the best surface roughness behaviour in all six FDM 3D printed parts analysed. With a maximum layer height of 0.3 mm, the surface roughness behaviour increased significantly by almost three hundred times. Again, this was because the maximum layer height of 0.3 mm required more time to cure for the crystallization of the thermoplastic filament material.

When measuring the direction of 45° (diagonally across building direction) and 90° (perpendicular to building direction), the difference of the surface roughness behaviour fluctuated within ~7 µm of one another, which is almost ~1 µm difference in the surface roughness behaviour to the inner faces due to study-state ambient temperature. Whereas, when measuring the direction of 0° (parallel to building direction), the surface roughness behaviour fluctuated within ~2 µm.

At 0.5 mm nozzle diameter for both 45° and 90°, the surface roughness decreased by almost 12.5% indicating that the surface finish improved from ~40 µm (at 0.3 mm layer height) to ~35 µm (at 0.2 mm layer height) until it reached ~22 µm when the layer height is 0.1 mm. At 0.3 mm nozzle diameter for both 45° and 90°, the surface roughness decreased by almost 60% indicating that the surface finishes improved from ~30 µm (at 0.2 mm layer height) to ~12 µm (at 0.1 mm layer height). At 0.2 mm nozzle diameter for both 45° and 90°, the surface finish reached ~12 µm when the layer height is 0.1 mm. On the other hand, at 0° measuring direction, all surface roughness behaviour was approximately the same for all nozzle diameter and layer height at around ~3 µm. The effect of nozzle diameter and layer height on the surface roughness can also be seen with naked-eye observation.

To conclude at outer faces, printed part no.5 represents the lowest average surface roughness behaviour with a total building time of almost two hours.

3.4. Measuring Direction *vs.* Average R_a at Inner Faces

Figure 10 demonstrates the measuring direction (0°, 45°, 90°) versus the average surface roughness, R_a, behaviour of six FDM 3D printed parts at different dependent and independent manufacturing process parameters. It is worth mentioning that each data point is an average value of four readings (four identical faces) of each printed sample for the inner faces.

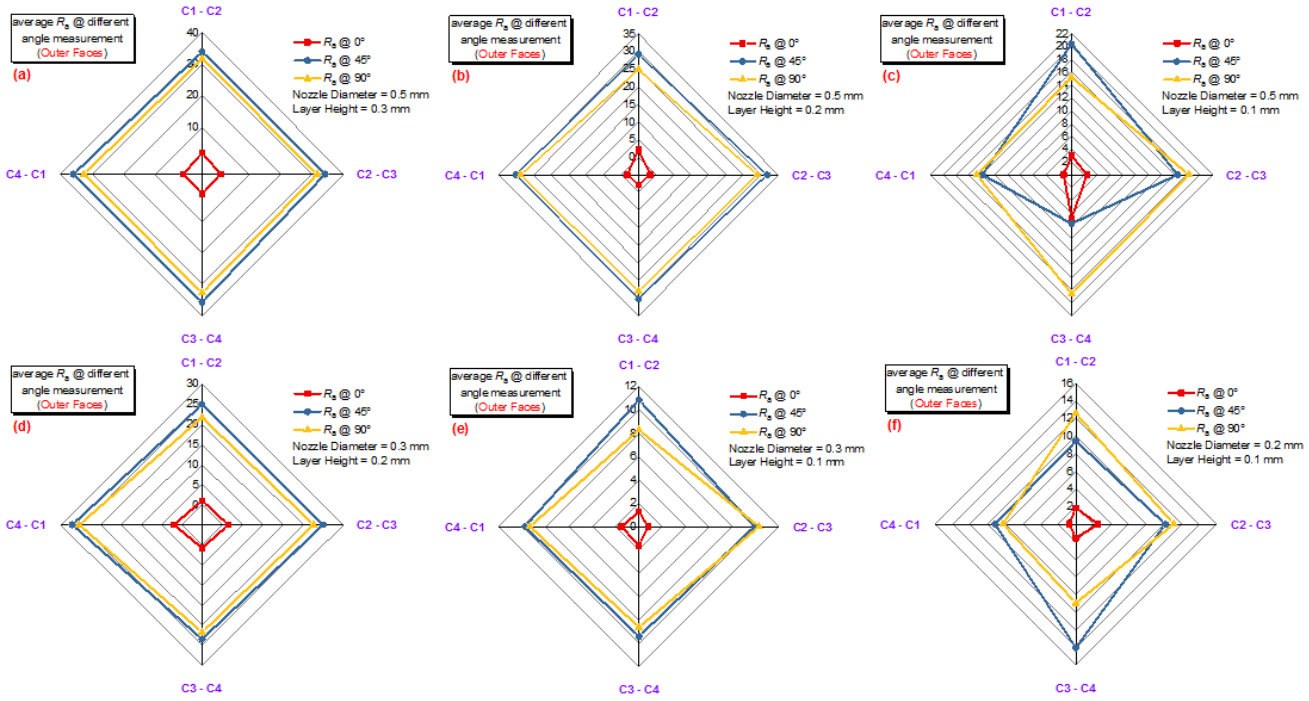

Figure 9. Surface roughness of outer faces at different angular measurement and different process parameters

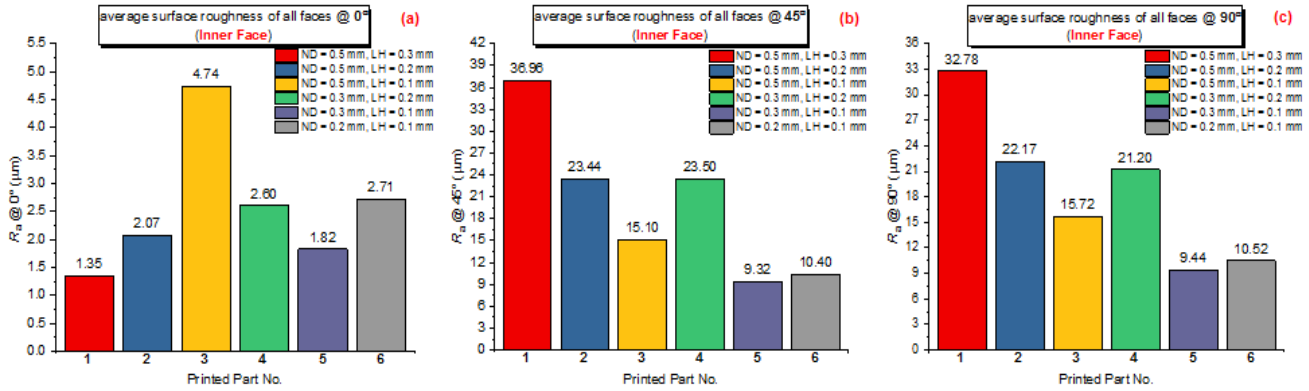

Figure 10. Average surface roughness of all faces at (a) 0° (b) 45° and (c) 90° angular measurement (inner faces)

At a 0° measuring direction, as shown in Figure 10(a), printed part no.1 represented the lowest average surface roughens behaviour at 1.35±0.27 µm when nozzle diameter and layer height were 0.5 mm and 0.3 mm, respectively. Whereas, printed part no.3 represented the highest average surface roughness behaviour at 4.74±2.19 µm when nozzle diameter and layer height were 0.5 mm and 0.1 mm, respectively. Also, at 0°, printed part no.1 has the lowest average R_a however at 45° and 90°, it shows otherwise indicating that the measuring direction plays a significant role in the surface roughness behaviour.

At a 45° measuring direction, as shown in Figure 10(b), printed part no.1 represented the highest average surface roughness behaviour at 36.96±0.51 µm when nozzle diameter and layer height were 0.5 mm and 0.3 mm, respectively. Whereas, printed part no.5 represented the lowest average surface roughness behaviour at 9.32±0.33 µm when nozzle diameter and layer height were 0.3 mm and 0.1 mm, respectively.

At a 90° measuring direction, as shown in Figure 10(c), printed part no.1 represented the highest average surface roughness behaviour at 32.78±0.79 µm when nozzle diameter and layer height were 0.5 mm and 0.3 mm, respectively. Whereas, printed part no.5 represented the lowest average surface roughness behaviour at 9.44±0.92 µm when nozzle diameter and layer height were 0.3 mm and 0.1 mm, respectively.

From the data presented in Figure 10, it can be concluded that measuring the angle of 90° is more suited for measuring the behaviour of the surface roughness compared to the other angles (0° and 45°). Based on these findings, the printed part no.5 (inner faces) shows the lowest average surface roughness behaviour when nozzle diameter and layer height were 0.3 mm and 0.1 mm, respectively.

3.5. Measuring Direction *vs.* Average R_a at Outer Faces

Figure 11 shows the measuring direction (0°, 45°, 90°) versus the average surface roughness behaviour of six FDM 3D printed parts at different dependent and independent manufacturing process parameters. It is worth mentioning that each data point is an average value of four readings (four faces) of each printed sample for the outer faces.

At a 0° measuring direction, as shown in Figure 11(a), printed part no.4 represented the lowest average surface roughness behaviour at 1.08±0.30 µm when nozzle diameter and layer height were 0.3 mm and 0.2 mm, respectively. Whereas, printed part no.3 represented the highest average surface roughness behaviour at 8.62±3.90 µm when nozzle diameter and layer height were 0.5 mm and 0.1 mm, respectively. Also, at 0°, printed part no.4 has the lowest average R_a however at 45° and 90°, it shows otherwise indicating that the measuring direction plays a significant role in the surface roughness behaviour.

At a 45° measuring direction, as shown in Figure 11(b), printed part no.1 represented the highest average surface roughness behaviour at 34.94±1.04 µm when nozzle diameter and layer height were 0.5 mm and 0.3 mm, respectively. Whereas, printed part no.5 represented the lowest average surface roughness behaviour at 9.98±0.61 µm when nozzle diameter and layer height were 0.3 mm and 0.1 mm, respectively.

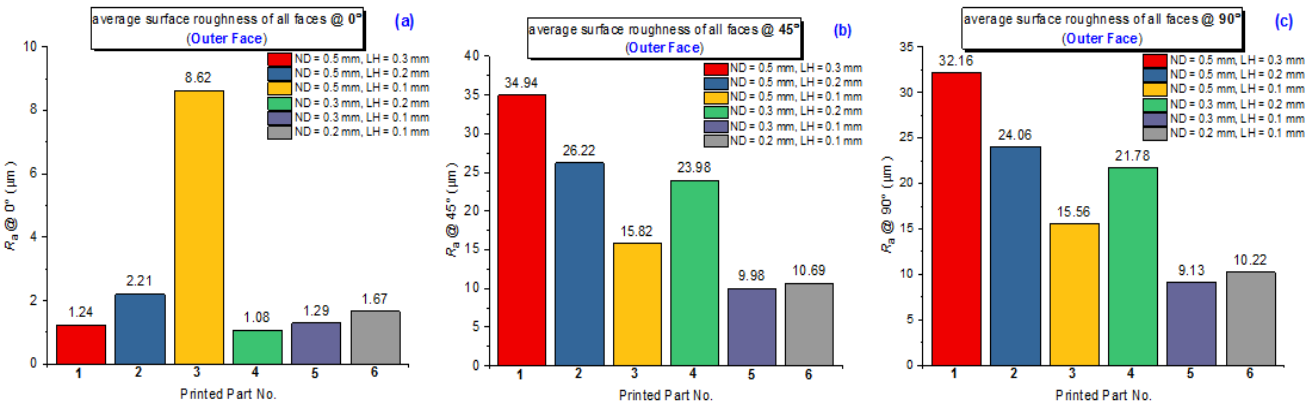

Figure 11. Average surface roughness of all faces at (a) 0° (b) 45° and (c) 90° angular measurement (outer faces)

At 90° measuring direction, as shown in Figure 11(c), printed part no.1 represented the highest average surface roughness behaviour at 32.16±0.61 µm when nozzle diameter and layer height were 0.5 mm and 0.3 mm, respectively. Whereas, printed part no.5 represented the lowest average surface roughness behaviour at 9.13±0.90 µm when nozzle diameter and layer height were 0.3 mm and 0.1 mm, respectively.

From the data presented in Figure 11, it can be said that measuring the angle of 90° is more suited for measuring the behaviour of the surface roughness compared to the other angles. Based on these findings, the printed part no.5 (outer faces) shows the lowest average surface roughness behaviour when nozzle diameter and layer height were 0.3 mm and 0.1 mm, respectively, which is consistent with the inner faces.

To conclude, the average surface roughness behaviour decreased by 29.1% in printed part no.5 at 0° from inner to outer faces indicating that the surface finish is rougher inside than outside due to solidification process and also by the assistance of surrounding heat provided by the nozzle temperature. However, at 45°, it increased by 7% from inner to outer faces and again decreased by 3% from inner to outer faces at 90°.

4. Concluding Remarks

In this work, with the desktop low-cost FDM 3D printer and PLA+ thermoplastic filament as the building material, six successful 0% infill density printed parts were straightforwardly manufactured and measured using a contact-type precision measuring instrument. No post-processing steps were taken to polish the printed parts. The optimal parameter setting for improving the surface roughness is obtained. The obtained data provides a convenient data set, which can be used to quantitively analyze and calculate the surface roughness behaviour and the profile distribution of printed parts under different conditions and the main partial conclusions of this study were the following:

- Measuring direction of 90° gives the most representative value of R_a distribution than other angles (0° and 45°) to derive data from.
- The decrease in nozzle diameter from 0.3 mm to 0.2 mm with decreasing layer height to 0.1 mm increases the build time of the printed parts no. 5 and no. 6 and feedstock thermoplastic filament material consumption significantly.
- In inner faces, the highest surface roughness behaviour was 36.96±0.51 µm (part no.1) at 45° measuring direction, and the lowest surface roughness behaviour was 1.35±0.27 µm (part no.1) at 0° measuring direction, when nozzle diameter and layer height were 0.5 mm and 0.3 mm, respectively.
- In outer faces, the highest surface roughness behaviour was 34.94±1.04 µm (part no.1) at 45° measuring direction, when nozzle diameter and layer height were 0.5 mm and 0.3 mm, respectively. However, the lowest surface roughness behaviour was 1.08±0.30 µm (part no.4) at 0° measuring direction, when nozzle diameter and layer height were 0.3 mm and 0.2 mm, respectively.
- As the high value of the surface roughness behaviour, the comparison between the inner and outer faces of all six FDM 3D printed parts configurations show some differences by almost ~2 µm (5%)
- As the low value of the surface roughness behaviour, the comparison between the inner and outer faces of all six FDM 3D printed parts configurations show some differences by almost ~0.27 µm (20%).

As a conclusion, we believe that the inner faces of 0% infill density printed parts were rougher than outer faces due to solidification process under the manufacturing process parameters mentioned earlier. So, the aim of this understanding is to explain the complex measuring direction and also represent in detail the effect of process parameters on the output response, especially as regards the printed part quality.

Conflicts of Interest

The authors declare that there is no conflict of interest involved during the preparation of this manuscript.

Funding Source

The authors received no financial support for the research and/or for the publication of this article.

References

[1] Kong, Y. L., et al., *3D Printed Bionic Nanodevices.* Nano today, 2016. 11(3): p. 330-350.

[2] Wang, X., et al., *3D printing of polymer matrix composites: A review and prospective.* Composites Part B: Engineering, 2017. 110: p. 442-458.

[3] Hull, C. W., *Apparatus for production of three-dimensional objects by stereolithography*. 1986, Google Patents.

[4] Pham, D. T. and R. S. Gault, *A comparison of rapid prototyping technologies.* International Journal of Machine Tools and Manufacture, 1998. 38(10-11): p. 1257-1287.

[5] Song, Y., et al., *Measurements of the mechanical response of unidirectional 3D-printed PLA.* Materials & Design, 2017. 123: p. 154-164.

[6] Mcloughlin, L., et al., *Virtual Sculpting and 3D Printing for Young People with Disabilities.* IEEE Computer Graphics and Applications, 2016. 36(1): p. 22-28.

[7] Joshi, S. C. and A. A. Sheikh, *3D printing in aerospace and its long-term sustainability.* Virtual and Physical Prototyping, 2015. 10(4): p. 175-185.

[8] Balashanmugam, N., et al., *STL-less based CAD/CAM Approach for Laser Scanning in Micro Stereo Lithography.* Procedia Materials Science, 2014. 5: p. 1466-1472.

[9] Fina, F., et al., *Selective laser sintering (SLS) 3D printing of medicines.* International Journal of Pharmaceutics, 2017. 529(1): p. 285-293.

[10] Derby, B., *Inkjet printing ceramics: From drops to solid.* Journal of the European Ceramic Society, 2011. 31(14): p. 2543-2550.

[11] Yan, J., I. Battiato, and G. Fadel, *Design of injection nozzle in direct metal deposition (DMD) manufacturing of thin-walled structures based on 3D models.* The International Journal of Advanced Manufacturing Technology, 2017. 91(1): p. 605-616.

[12] Alafaghani, A. a., et al., *Experimental Optimization of Fused Deposition Modelling Processing Parameters: A Design-for-Manufacturing Approach*. Procedia Manufacturing, 2017. 10: p. 791-803.

[13] Yuen, P. K., *Embedding objects during 3D printing to add new functionalities.* Biomicrofluidics, 2016. 10(4): p. 044104.

[14] Wang, T.-M., J.-T. Xi, and Y. Jin, *A model research for prototype warp deformation in the FDM process.* The International Journal of Advanced Manufacturing Technology, 2007. 33(11): p. 1087-1096.

[15] Ahn, S.-H., et al., *Anisotropic material properties of fused deposition modeling ABS.* Rapid Prototyping Journal, 2002. 8(4): p. 248-257.

[16] Roberson, D., et al., *Expanding the applicability of FDM-type technologies through materials development.* Rapid Prototyping Journal, 2015. 21(2): p. 137-143.

[17] Tran, P., et al., *Bimaterial 3D printing and numerical analysis of bio-inspired composite structures under in-plane and transverse loadings.* Composites Part B: Engineering, 2017. 108: p. 210-223.

[18] Melnikova, R., A. Ehrmann, and K. Finsterbusch, *3D printing of textile-based structures by Fused Deposition Modelling (FDM) with different polymer materials.* IOP Conference Series: Materials Science and Engineering, 2014. 62(1): p. 012018.

[19] Alafaghani, A. a., A. Qattawi, and M. A. Ablat, *Design Consideration for Additive Manufacturing: Fused Deposition Modelling*. Open Journal of Applied Sciences, 2017. 7(6): p. 291-318.

[20] Martin, O. and L. Avérous, *Poly(lactic acid): plasticization and properties of biodegradable multiphase systems.* Polymer, 2001. 42(14): p. 6209-6219.

[21] Hongdilokkul, P., et al., *A study on properties of PLA/PBAT from blown film process.* IOP Conference Series: Materials Science and Engineering, 2015. 87(1): p. 012112.

[22] Alsoufi, M. S. and A. E. Elsyeed, *Warping Deformation of Desktop 3D Printed Parts Manufactured by Open Source Fused Deposition Modeling (FDM) System.* International Journal of Mechanical and Mechatronics Engineering, 2017. 17(4): p. 7-16.

[23] Sun, Q., et al., *Effect of processing conditions on the bonding quality of FDM polymer filaments.* Rapid Prototyping Journal, 2008. 14(2): p. 72-80.

[24] Yang, Y., et al., *3D printing of shape memory polymer for functional part fabrication.* The International Journal of Advanced Manufacturing Technology, 2016. 84(9): p. 2079-2095.

[25] Lee, C.S., et al., *Measurement of anisotropic compressive strength of rapid prototyping parts.* Journal of Materials Processing Technology, 2007. 187(Supplement C): p. 627-630.

[26] Sood, A.K., R.K. Ohdar, and S.S. Mahapatra, *Improving dimensional accuracy of Fused Deposition Modelling processed part using grey Taguchi method.* Materials & Design, 2009. 30(10): p. 4243-4252.

[27] Thrimurthulu, K., P.M. Pandey, and N. Venkata Reddy, *Optimum part deposition orientation in fused deposition modeling.* International Journal of Machine Tools and Manufacture, 2004. 44(6): p. 585-594.

[28] Vega, V., et al., *The Effect of Layer Orientation on the Mechanical Properties and Microstructure of a Polymer*. Journal of Materials Engineering and Performance, 2011. 20(6): p. 978-988.

[29] Chuang, K.C., et al., *A Fully Nonmetallic Gas Turbine Engine Enabled by Additive Manufacturing, Part II: Additive Manufacturing and Characterization of Polymer Composites.* 2015, NASA: USA.

[30] Tekinalp, H.L., et al., *Highly oriented carbon fiber–polymer composites via additive manufacturing.* Composites Science and Technology, 2014. 105: p. 144-150.

[31] Nikzad, M., S.H. Masood, and I. Sbarski, *Thermo-mechanical properties of a highly filled polymeric composites for Fused Deposition Modeling.* Materials & Design, 2011. 32(6): p. 3448-3456.

[32] Alsoufi, M. S. and T. M. Bawazeer, *Quantifying assessment of touch-feel perception: an investigation using stylus base equipment and self-touch (human fingertip).* Umm Al-Qura University: Journal of Engineering and Architecture, 2015. 1(1): p. 1-16.

[33] Alsoufi, M. S. and T. M. Bawazeer, *The Effect of Aggressive Biological Materials on a Painted Automotive Body Surface Roughness.* American Journal of Nano Research and Applications, 2015. 3(2): p. 17-26.

[34] Suker, D. K., et al., *Studying the Effect of Cutting Conditions in Turning Process on Surface Roughness for Different Materials.* World Journal of Research and Review (WJRR), 2016. 2(4): p. 16-21.

[35] Alsoufi, M. S., et al., *Experimental Study of Surface Roughness and Micro-Hardness Obtained by Cutting Carbon Steel with Abrasive WaterJet and Laser Beam Technologies.* American Journal of Mechanical Engineering, 2016. 4(5): p. 173-181.

[36] Bawazeer, T. M., et al., *Effect of Aqueous Extracts of Salvadora Persica "Miswak" on the Acid Eroded Enamel Surface at Nano-Mechanical Scale.* Materials Sciences and Applications, 2016. 7(11): p. 754-771.

[37] Alsoufi, M. S., et al., *Surface Roughness and Knoop Indentation MicroHardness Behavior of Aluminium Oxide (Al2O3) and Polystyrene ($C_8H_8)_n$ Materials* International Journal of Mechanical & Mechatronics Engineering 2016. 16(6): p. 43-49.

[38] Alsoufi, M. S., *State-of-the-Art in Abrasive Water Jet Cutting Technology and the Promise for Micro- and Nano-Machining.* International Journal of Mechanical Engineering and Applications, 2017. 5(1): p. 1-14.

[39] Alsoufi, M. S., et al., *Influence of Abrasive Waterjet Machining Parameters on the Surface Texture Quality of Carrara Marble.* Journal of Surface Engineered Materials and Advanced Technology, 2017. 7(2): p. 25-37.

[40] Alsoufi, M. S., et al., *Abrasive WaterJet Machining of Thick Carrara Marble: Cutting Performance vs. Profile, Lagging and WaterJet Angle Assessments.* Materials Sciences and Applications, 2017. 8(5): p. 361-375.

[41] Alsoufi, M. S., et al., *The Effect of Detergents on the Appearance of Automotive Clearcoat Systems Studied in an Outdoor Weathering Test* Materials Sciences and Applications, 2017. 8(7): p. 521-536.

[42] Dong, W.P., P.J. Sullivan, and K.J. Stout, *Comprehensive study of parameters for characterizing three-dimensional surface topography I: Some inherent properties of parameter variation.* Wear, 1992. 159(2): p. 161-171.

[43] Dong, W.P., P.J. Sullivan, and K.J. Stout, *Comprehensive study of parameters for characterizing three-dimensional surface topography II: Statistical properties of parameter variation.* Wear, 1993. 167(1): p. 9-21.

[44] Dong, W.P., P.J. Sullivan, and K.J. Stout, *Comprehensive study of parameters for characterizing three-dimensional surface topography III: parameters for characterising amplitude and some functional properties.* Wear, 1994. 178(1): p. 29-43.

[45] Dong, W.P., P.J. Sullivan, and K.J. Stout, *Comprehensive study of parameters for characterising three-dimensional surface topography: IV: Parameters for characterising spatial and hybrid properties.* Wear, 1994. 178(1): p. 45-60.

[46] Thomas, T.R., *Characterization of surface roughness.* Precision Engineering, 1981. 3(2): p. 97-104.